

A Closed-Loop Controller for Cable-Driven Hyper-Redundant Manipulator with Joint Angle Sensors*

Baibo Wu¹, Lingyun Zeng¹, Yang Zheng¹, Shu'an Zhang², Xiangyang Zhu¹ and Kai Xu¹

¹State Key Laboratory of Mechanical System and Vibration
School of Mechanical Engineering

²RII Lab (Lab of Robotics Innovation and Intervention)
UM-SJTU Joint Institute

Shanghai Jiao Tong University
Shanghai, China

{wubaibo, me_maxqi, zzyy0608, jimmyonthego, mexyzhu & k.xu} @ sjtu.edu.cn

Abstract - A cable-driven hyper-redundant manipulator is especially suited for manipulations in confined spaces. In most of the existing approaches, a controller is often designed to actuate the joints by pulling the corresponding cables without the feedback from remote sensors at the joints. The un-modeled elongations of these cables due to unknown tensions often cause a decrease in control precision. To improve the performance of such a manipulator, this paper presents an investigation where miniature potentiometers are integrated into the joints for angle feedback. Furthermore, a puller-follower controller is developed to control the three cables of a universal joint for not only closed-loop joint angle control but also cable tension preservation. Applying the Hooke's Law, the cable tension is represented by its deformation. In this way, the controller is designed to realize both the desired angles and the cable deformations, without force sensing on the cables. Finally, experiments on a single joint and multiple joints were conducted to verify the effectiveness of this proposed controller.

I. INTRODUCTION

Slim and long hyper-redundant manipulator is especially suited for manipulations in confined spaces, such as inspection, maintenance and other complex tasks in nuclear [1], aerospace [2, 3], and medical applications [4]. Due to its highly redundant kinematics, these hyper-redundant manipulators have distinctive advantages over traditional industrial robots, such as larger workspace, singularity avoidance, distal dexterity, etc.

A hyper-redundant manipulator is usually an articulated structure with its links serially connected by multiple joints. Investigation on the hyper-redundant manipulators can be dated back to the 1960s when Anderson and Horn developed the hyper-redundant Tensor Arm manipulator [5]. Since then, many hyper-redundant manipulators with different structures have been developed. They are classified as follows.

1) Module joints: the manipulator consists of serially connected modular joints with actuators integrated inside [6-8]. In this way, the joints can be controlled in a decoupled way. However, modular joints are usually complex. The distal modules become payload of the proximal joints. This hence limits the total number of the links.

- 2) Articulated joints with proximal actuation: the manipulator is constructed with serial links and revolute joints that are actuated by multiple cables with proximally arranged motors. The joints can be actuated in an independent manner, where a joint is actuated by a pair of cables [9, 10], or in a dependent manner, where a 2-DoF (Degree of Freedom) universal joint is driven by three cables [3, 11].
- 3) Continuum joints: the manipulator is composed of stacked continuum segments whose motion is realized by the deflection [12-16], rather than articulated joints. Continuum joints bring advantages such as compliance for safe interaction with environments. There also are noticeable limitations such as low stiffness and difficulty in sensor integration in the joints. This can reduce the motion accuracy and payload capability.

In the cases where a pair of cables actuates a revolute joint, the antagonistic arrangement and tension control of the cables are the main challenges in the controller design. Several approaches have been proposed, such as the position and force controller [17], the antagonistic impedance controller [18], and the puller-follower controller [19]. On the other hand, in the cases where a 2-DOF universal joint is driven by three cables, the joints are usually actuated in an open-loop manner [3, 11]. Due to the absence of joint feedbacks, the errors originated from the cable elongation are difficult to measure and compensate accordingly. Even with a feedforward dynamic controller implemented for controlling both the joint angle and the cable tension [3], high accuracy is still difficult to achieve since the joint angles are calculated iteratively from the kinematics, rather than obtained from direct measurements.

In order to achieve a higher accuracy, this paper presents a design of a cable-driven hyper-redundant manipulator (CDHM) with joint angle sensors integrated. Using the feedback signals, a closed-loop position controller, inspired by the puller-follower controller in [19], is then proposed with the following features:

- The joint angle is directly obtained from the angle sensor and the cable tension is represented by the cable elongation according to the Hooke's Law;

* This work was supported in part by the National Natural Science Foundation of China (Grant No. 51435010, Grant No. 51722507 and Grant No. 91648103), and in part by the National Key R&D Program of China (Grant No. 2017YFC0110800).

- The three antagonistic cables is regulated with the proposed puller-follower strategy which also maintains cable tension;
- No force sensors are needed and the motors all work in the position-servo mode.

With this proposed closed-loop controller, the puller cables are actuated according to the cable-joint kinematics while the follower cables are actuated according to the desired cable elongation that is solved via the cable elasticity and the unilateral actuation (a.k.a., only pulling is allowed). To verify the effectiveness of this controller, both single-joint actuation and six-joint actuation experiments were conducted. The results of the single-joint and six-joint motions show that the closed-loop control of the joint angles were realized, while the cable deformations were properly maintained.

The paper is organized as follows. Section II presents a description of the CDHM, while the kinematics is derived in Section III. The controller is proposed in Section IV. The experimental characterizations are reported in Section V with the conclusions and future work summarized in Section VI.

II. STRUCTURE OF CDHM

The CDHM structure is shown in Fig. 1, including an actuation box, a snake arm and a linear actuator.

The snake arm has 12 rigid links serially connected by 12 universal joints with an overall length of 1.8 m. Each universal joint allows motion ranges of 30° in the yaw and pitch directions. The joint motion ranges will facilitate the intended inspection motions in confined spaces. Two miniature angle sensors are installed on the two shafts of each universal joint to measure the joint angles.

Each universal joint is driven by three cables that are routed through the lumens in the proximal links. A total number of 36 leadscrews actuated by the servomotors in the actuation box provide actuation to each cable in the snake arm. Finally, the actuation box along with the snake arm is loaded on the linear actuator that provides the feeding motion for the snake arm.

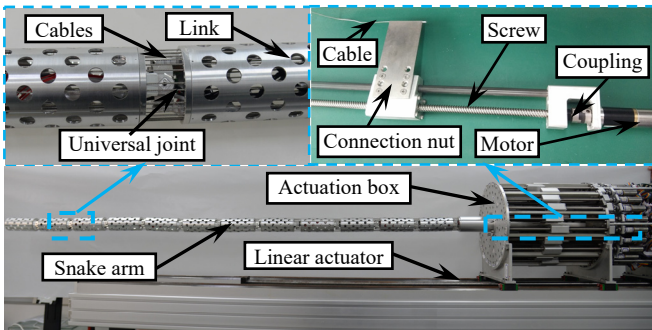


Fig. 1. A cable-driven hyper-redundant manipulator with the feedback sensors integrated at the universal joints

The detailed structure of the universal joint is shown in Fig. 2. Each universal joint consists of a connection block and two guiding disks with 36 evenly distributed holes. The actuation cables are routed through the holes and are fixed to the corresponding links (namely, the arm tube). To measure the joint angles, two sensors are integrated in the universal joint

with the sensor body fixed to the connection block and the sensor input hole connected with the connection shaft. The dimension of the sensor, as detailed in Section IV.A, is $15 \text{ mm} \times 11 \text{ mm} \times 2.8 \text{ mm}$, which enables its arrangement in the joint without interfering with the cables.

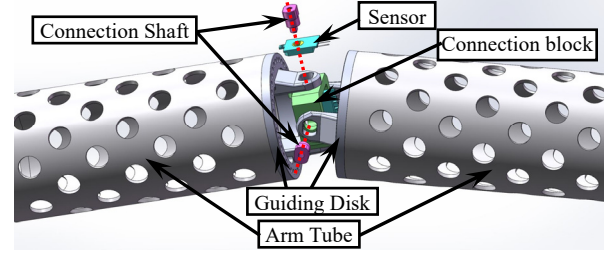


Fig. 2. Universal joint with two angle sensors

III. KINEMATICS

Nomenclature and coordinates are defined in Section III.A and the kinematics is derived in Section III.B.

A. Nomenclature and Coordinates

The coordinates are defined as follows, referring to Fig. 4, while the nomenclature is summarized in Table. I.

TABLE I
NOMENCLATURE USED IN THE KINEMATICS MODEL

Symbol	Definition
i	Index of the universal joints. $i = 1, 2, \dots, 12$.
j	Index of the cables and motors. $j = 1, 2, \dots, 36$.
θ_{jm}, l_{jm}	Angle of the j^{th} motor and actuation length of the j^{th} cable.
α_i, β_i	Actual yaw and pitch angle of the i^{th} joint
α_{id}, β_{id}	Desired yaw and pitch angle of the i^{th} joint
l_{ij}	Length of the j^{th} cable within the i^{th} joint.
l_j	Total length of the j^{th} cable spanning all the routed joints.
ϵ_j	Elongation of the j^{th} cable, relative to the initial status.
$\mathbf{P}_{ij1}, \mathbf{P}_{ij2}$	Position of the intersection points of the j^{th} cable with the proximal and distal disks in the i^{th} joint.
f_b	The displacement of the linear actuator.
φ_j	The distribution angle of the j^{th} cable. $\varphi_j = (j-1)\pi/18$.
r, h	The distribution radius of the cable routing holes and the height of the guiding disk.
L_{tube}	The length of the arm tubes

- **Proximal Disk Coordinate** $\{p, i\} \equiv \{\hat{\mathbf{x}}_{p,i}, \hat{\mathbf{y}}_{p,i}, \hat{\mathbf{z}}_{p,i}\}$ is attached to the center of the proximal disk in the i^{th} universal joint. $\hat{\mathbf{z}}_{p,i}$ is parallel to the rotating shaft between the proximal disk and the connection block.
- **Universal Joint Coordinate** $\{u, i\} \equiv \{\hat{\mathbf{x}}_{u,i}, \hat{\mathbf{y}}_{u,i}, \hat{\mathbf{z}}_{u,i}\}$ is attached to the center of the connection block in the i^{th} universal joint. $\hat{\mathbf{y}}_{u,i}, \hat{\mathbf{z}}_{u,i}$ are aligned with the rotating shafts that connecting the proximal and the distal disk, respectively.
- **Distal Disk Coordinate** $\{d, i\} \equiv \{\hat{\mathbf{x}}_{d,i}, \hat{\mathbf{y}}_{d,i}, \hat{\mathbf{z}}_{d,i}\}$ is attached to the center of the distal disk in the i^{th} universal joint. $\hat{\mathbf{z}}_{d,i}$ is parallel to the rotating shaft between the connection block and the distal disk.

B. Kinematics

Kinematics of the CDHM involves various mapping between the motor space, the cable space, the joint space, and the task space, as shown in Fig. 3.

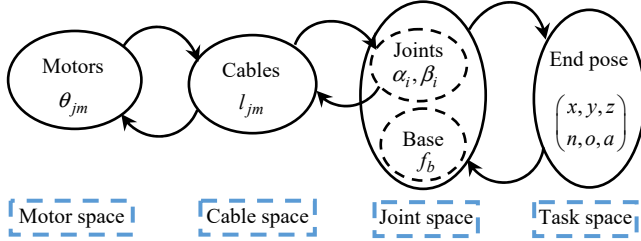


Fig. 3. The kinematics mapping of the CDHM

The actuation kinematics mapping between the motor angle and the cable length follows a simple proportional linear model, which is straightforward.

Three cables actuate the i^{th} universal joint as shown in Fig. 4. The mapping from the cable lengths to the joint angles can be solved analytically [11] or numerically [3]. In the proposed controller, the mapping from the joint angles to the cable lengths is utilized. With the joint angle feedback available, the cable elongation, which leads to the actuation inaccuracy, can be calculated as the difference between the change of the total cable length and the motor actuation length.

The direct mapping from the joint space to the task space is straightforward. The inverse mapping is obviously not unique due to kinematics redundancy. The inverse kinematics can be solved via various approaches, such as the modified modal method [20] or the tip following algorithm [21].

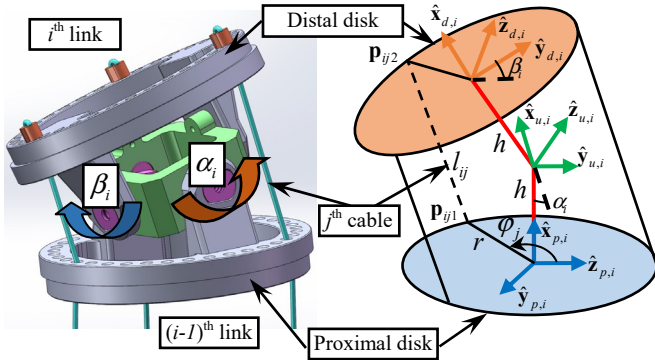


Fig. 4. The structure of the i^{th} universal joint

The homogeneous coordinates of point \mathbf{p}_{ij1} and \mathbf{p}_{ij2} can be expressed respectively in $\{p, i\}$ and $\{d, i\}$ as:

$$\begin{aligned} {}^{p,i}\mathbf{p}_{ij1} &= \begin{bmatrix} 0 & -r \cdot \sin \varphi_j & r \cdot \cos \varphi_j & 1 \end{bmatrix}^T \\ {}^{d,i}\mathbf{p}_{ij2} &= \begin{bmatrix} 0 & r \cdot \cos \varphi_j & r \cdot \sin \varphi_j & 1 \end{bmatrix}^T \end{aligned} \quad (1)$$

The transformation from $\{p, i\}$ to $\{u, i\}$ and from $\{u, i\}$ to $\{d, i\}$ can be expressed respectively as:

$$\begin{aligned} {}^{p,i}\mathbf{T}_{u,i} &= \text{Trans}(\hat{\mathbf{x}}, h) \cdot \text{Rot}(\hat{\mathbf{z}}, \alpha_i) \cdot \text{Rot}(\hat{\mathbf{x}}, \pi/2) \\ {}^{u,i}\mathbf{T}_{d,i} &= \text{Rot}(\hat{\mathbf{z}}, \beta_i) \cdot \text{Trans}(\hat{\mathbf{x}}, h) \end{aligned} \quad (2)$$

Then, the transformation from $\{p, i\}$ to $\{d, i\}$ is derived accordingly as follows.

$${}^{p,i}\mathbf{T}_{d,i} = {}^{p,i}\mathbf{T}_{u,i} \cdot {}^{u,i}\mathbf{T}_{d,i} \quad (3)$$

Thus, the point \mathbf{p}_{ij2} can be expressed in $\{p, i\}$ as:

$$\begin{aligned} {}^{p,i}\mathbf{p}_{ij2} &= {}^{p,i}\mathbf{T}_{d,i} \cdot {}^{d,i}\mathbf{p}_{ij2} \\ &= \begin{bmatrix} -r \cdot c\alpha_i s\beta_i c\varphi_j + r \cdot s\alpha_i s\varphi_j + h \cdot c\alpha_i c\beta_i + h \\ -r \cdot s\alpha_i s\beta_i c\varphi_j - r \cdot c\alpha_i s\varphi_j + h \cdot s\alpha_i c\beta_i \\ r \cdot c\beta_i c\varphi_j + h \cdot s\beta_i \\ 1 \end{bmatrix} \end{aligned} \quad (4)$$

Where s and c are short for \sin and \cos , respectively.

And the cable length in the i^{th} universal joint is the distance between the \mathbf{p}_{ij1} and \mathbf{p}_{ij2} points.

$$l_j = \left| {}^{p,i}\mathbf{p}_{ij2} - {}^{p,i}\mathbf{p}_{ij1} \right| = f_j(\alpha_i, \beta_i, \varphi_j) \quad (5)$$

Using Eq. (5), the length of the j^{th} cable through the i^{th} universal joint can be calculated with the parameters $\alpha_i, \beta_i, \varphi_j$.

In the CDHM, the arrangements of the relative coordinate frames are shown in Fig. 5.

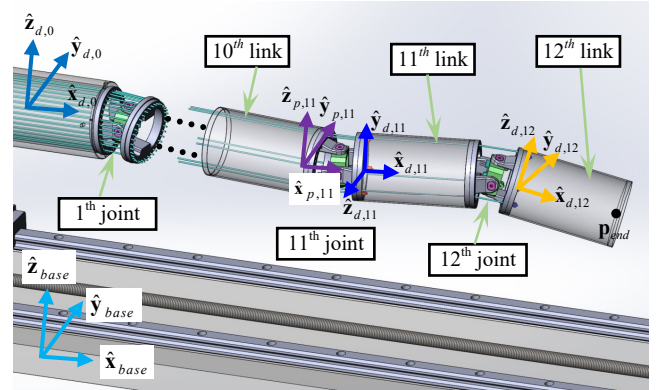


Fig. 5. The coordinate frames in the CDHM

The length of the j^{th} cable, which actuates the i^{th} joint, is a result of passing all the proximal joints as follows.

$$l_j = \sum_{k=1}^i l_{kj} = f_j(\alpha_1, \beta_1, \alpha_2, \beta_2, \dots, \alpha_i, \beta_i, \varphi_j) \quad (6)$$

With the joint angles, the homogeneous transformation from $\{d, 0\}$ to $\{d, 12\}$ is derived as follows.

$${}^{d,0}\mathbf{T}_{d,12} = \prod_{i=1}^{12} ({}^{d,i-1}\mathbf{T}_{p,i} \cdot {}^{p,i}\mathbf{T}_{d,i}) \quad (7)$$

Where ${}^{d,i-1}\mathbf{T}_{p,i} = \text{Trans}(\hat{\mathbf{x}}, L_{\text{tube}})$, ${}^{p,i}\mathbf{T}_{d,i}$ is as in Eq. (3) which differs in the odd or even indexed joint due to the different arrangement of the universal joint.

Combining with the motion of the linear actuator, the end position of the CDHM can be derived as:

$${}^{\text{base}}\mathbf{p}_{\text{end}} = {}^{\text{base}}\mathbf{T}_{d,0} \cdot {}^{d,0}\mathbf{T}_{d,12} \cdot {}^{d,12}\mathbf{p}_{\text{end}} \quad (8)$$

Where ${}^{d,12}\mathbf{p}_{\text{end}}$ is a constant vector representing the location of the end-effector on the 12^{th} link.

IV. PULLER-FOLLOWER CLOSED-LOOP CONTROLLER

Each joint of the CDHM is a 2-DoF universal one, which is actuated by three cables. Miniature angle sensors are integrated in the joints for achieving better motion accuracy. A puller-follower controller is designed for both closed-loop joint

angle control and cable tension regulation. The details of angle sensor integration are presented in Section IV. A, while the puller-follower controller is presented in Section IV. B.

A. Joint Angle Sensor

The angle sensor is a potentiometer from by muRata Inc. (SV01A103AEA01B00) with a sensing range of 333.3° . An acquisition board was designed and fabricated as shown in Fig. 6(a). The acquisition board include an operational amplifier chip (OPA4377AIPWR by TI Inc.) with four channels, a CAN (Controller Area Network) transceiver (SN65HVD1050DR by TI Inc.) and a microcontrollers F103 (STM32F103 by STMicroelectronics, Inc.).

As the motion range of a single joint in the CDHM is 30° , the angle's resolution is improved to 0.02° per bit after the amplification. Then, the digital signals from the ADCs (Analog-to-Digital Converters) are filtered by the low-pass filters before transmitting to the controller.

The relationship between the angle and ADC value may vary among different potentiometers and acquisition boards, and thus experimental calibrations are necessary. During the calibration, the actual angle of potentiometer is realized by a Maxon DCX16L servomotor with the GPX-16 gearhead and the ENX16 encoder, as shown in Fig. 6(b).

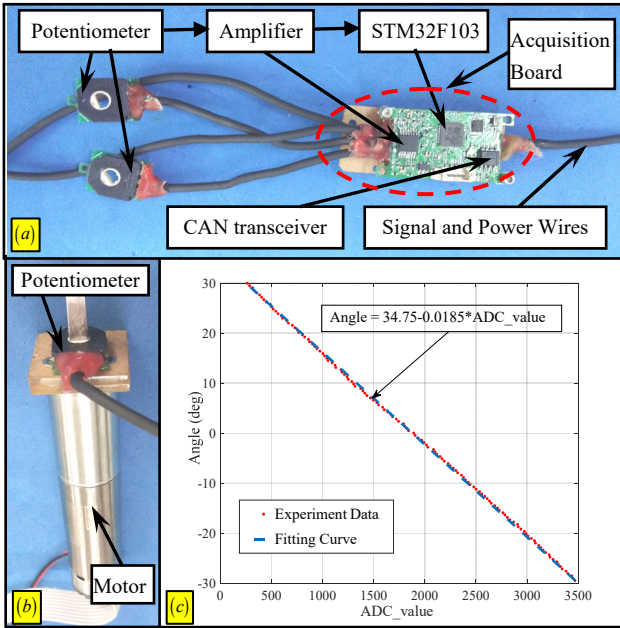


Fig. 6. (a) The angle sensors and the acquisition board; (b) the sensor calibration setup, (c) the calibration experimental results

A total of 24 sensors in the CDHM are calibrated one by one. The fitted curve of one sensor is shown in Fig. 6(c) with the ADC value approximately linear with the rotating angle.

B. Puller-Follower Controller

As the three cables for the universal joint are coupled and antagonistic, the tension on one cable can be influenced by the other cables. The deformation status of the three cables are shown in Fig. 7 when only the joint angles are controlled in a closed-loop mode without controlling the cable tensions. The cables gradually become slack. Inspired by the puller-follower

control in [19], a puller-follower controller for the 2-DoF universal joint is hence proposed to control both the joint angles and regulate cable tensions.

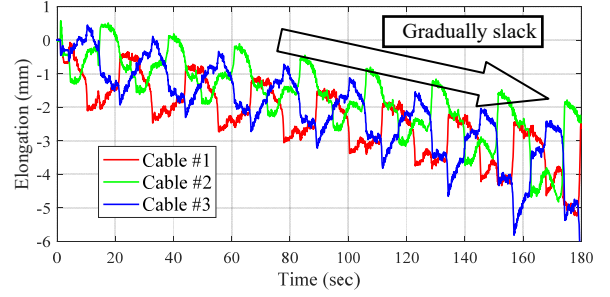


Fig. 7. Gradual slackness without the proposed cable tension control

The puller-follower controller for the i^{th} universal joint is illustrated in Fig. 8. There are two control objectives: i) the desired joint angles $(\alpha_{id}, \beta_{id})$, and ii) the desired cable deformation ε_{jd} which represents the desired tension. Two proportional controllers are used for the two objectives with the control parameters P_θ and P_ε . The actual joint angles (α_i, β_i) are measured by the two miniature angle sensors. The cable's elongation is calculated as follows.

$$\varepsilon_j = l_{jm} - dl_{j\theta} \quad (9)$$

Where $dl_{j\theta} = l_{j,act}^0 - l_{j,act}$ is the length change of the j^{th} cable relative to the initial status.

The kinematics from the joint angles to the cable lengths as in Section III.B is implemented here to calculate the cable lengths with the desired and actual joint angles.

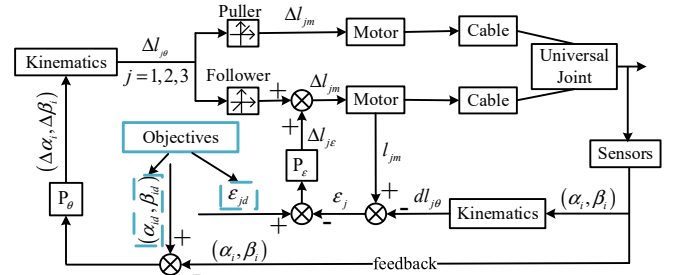


Fig. 8. Puller-follower controller for the i^{th} joint.

The puller and follower roles are identified by the driving length $\Delta l_{j\theta} > 0$ and $\Delta l_{j\theta} < 0$, respectively. And the cable actuations are set as in Eq. (10) with the puller cables leading the joint motion while the follower cables maintaining a proper cable tension. What's more, a constraint is attached to the follower cables as specified in Eq. (11) to ensure that the follower cable is still in the following status:

$$\Delta l_{jm} = \begin{cases} \Delta l_{j\theta}, & \Delta l_{j\theta} \geq 0 \\ \Delta l_{j\theta} + \Delta l_{je}, & \Delta l_{j\theta} < 0 \end{cases} \quad (10)$$

$$\Delta l_{je} = \begin{cases} P_\varepsilon \cdot (\varepsilon_j - \varepsilon_{jd}), & P_\varepsilon \cdot (\varepsilon_j - \varepsilon_{jd}) < -0.5 \cdot \Delta l_{j\theta} \\ -0.5 \cdot \Delta l_{j\theta}, & \text{else} \end{cases} \quad (11)$$

Using the proposed puller-follower control, the follower cable(s) will converge to the desired deformation ε_{jd} gradually and the tension of the puller cable(s) will be restricted. What's

more, two dead zone parameters are set for the angles (α_i, β_i) to suppress the sensing noises. In the proposed controller, the motors all work in position-servo mode, even though they constantly switch between the puller and the follower roles.

V. EXPERIMENTS AND RESULTS

A distributive communication infrastructure is designed with both UDP (User Datagram Protocol) communication via LAN (Local Area Network) and CAN communications, as shown in Fig. 9.

Four F407 microcontrollers (STM32F407 by ST Inc.) are deployed here to transmit and process the signals between an IPC (Industrial Personal Computer) and acquisition board motor drives (EPOS 36/2 by Maxon Inc.) and F103. For the communication between IPC and F407, the UDP broadcast and unicast are used to send and receive signals, respectively. Using this structure, the puller-follower algorithm is applied with its control frequency up to 100Hz.

Before the following experiments, all the actuation cables are pre-tightened initially by controlling the actuation current of their corresponding motors.

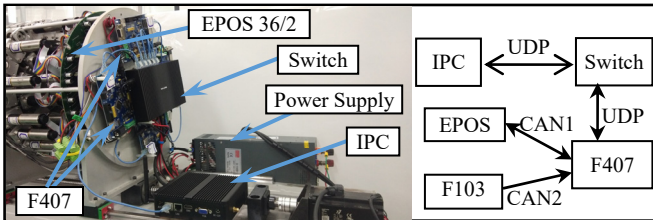


Fig. 9. Communication infrastructure of the CDHM

A. Single-joint Experimentation

The arrangement of the three cables in a joint is shown in Fig. 10(a). As shown in Fig. 10(b), the angle α_1 changes from 0° to 10° . The cables #1, #3 act as the puller cables with the cable #2 as the follower cable, which is the same working mode when angle β_1 changes from 0° to 10° .

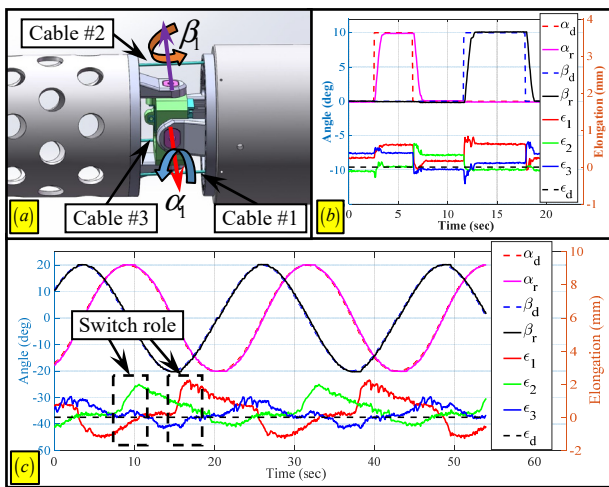


Fig. 10. Single-joint experimentation: (a) arrangement of the three cables, (b) the step responses, and (c) trajectory following

From the Fig. 10 (b), the deformation of cable #2 is converged to the desired deformation (zero relative to the initial status), which in turn limits the tension of cable #1 and #3. And the result is similar when angle β_1 changes from 0° to 10° , with the joint angles and elongations controlled simultaneously.

The result of a trajectory following is shown in Fig. 10(c). As the motion direction changed, the puller or the follower roles are switched among the three cables. The result shows that the joint angles follow the desired angles with the deformation of cables converged to the desired deformation. The gradual slackness as in Fig. 7 does not occur.

B. Multi-joint Experimentation

A six-joint experimentation was then conducted to verify the effectiveness and the stability of the proposed puller-follower controller. The desired joint angles are set sequentially for each joint from 0° to 10° . As in Fig. 11(a), the actual angles of each joint follow the desired angles from 0° to 10° and finally stabilize at 10° . The angle errors caused by the interaction between the joints are compensated with the feedbacks from the angle sensors. What's more, the maximum or minimum deformation of all 18 cables is maintained within ± 2 mm relative to the initial status, as shown in Fig. 11(b), avoiding slackness or excessive cable tensions.

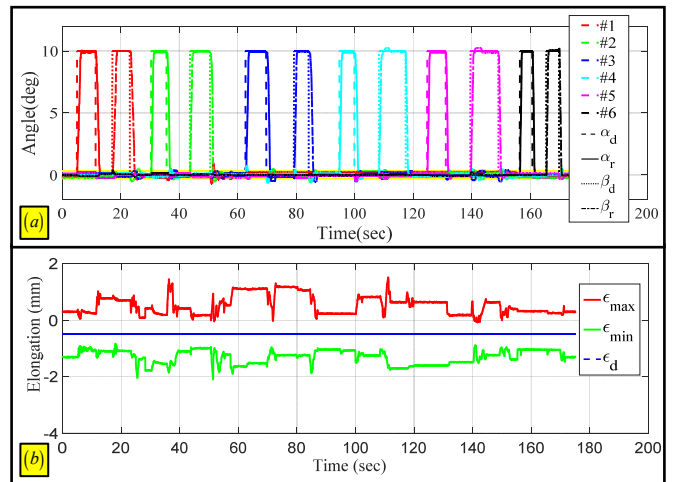


Fig. 11. Six-joint experimentation: (a) angle following curve of each joint (the color indicates the joint index, the line style indicates the actual/desired joint angles) (b) maximum and minimum deformations of the 18 cables

Then the CDHM was controlled to follow a curved trajectory, combining with the feeding motion from the linear actuator. As shown in Fig. 12, the preplanned trajectory is represented by the black lines and the color markers. The desired joint angles of the CDHM are planned using the tip-follow algorithm as in [21].

The tip of the CDHM arrived at the six marker points sequentially as shown from Fig. 12(a to f). The final shape of the snake arm matched well with the preplanned trajectory. What's more, the tensions of all the cables were kept in a safe range during the whole process, verifying the effectiveness of this proposed controller.

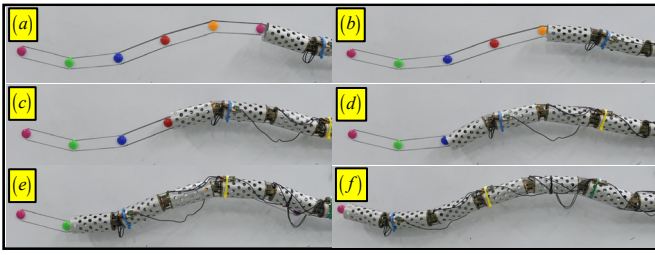


Fig. 12. Motion snapshots of following a curved trajectory.

VI. CONCLUSIONS AND FUTURE WORK

This paper proposes a closed-loop controller for a CDHM with the feedbacks of the joint angles, providing a solution to control the joint angles precisely as well as regulate the cable tensions. The angle sensors are integrated in the CDHM to measure the angles of the universal joints, while the cable tensions are represented by the cable deformations that can be obtained from the kinematics model. A puller-follower controller is then proposed to realize the desired joint angle as well as regulate proper cable deformation.

Both single-joint and multi-joint experimentations show that the joint angles can be controlled to follow the desired trajectories in a closed-loop manner and the tension of each cable was maintained in a safe range. What's more, the following of a curved trajectory illustrates the capacity of this controller to perform complex tasks.

Future works mainly include two aspects. First, the precision of angle sensor shall be improved to realize more precise manipulation in confined spaces. Second, the proposed controller should be improved to realize a shorter settling time. The current settling time on the order of a few seconds can cause the manipulator to oscillate while following a fast changing trajectory.

REFERENCES

- [1] R. Buckingham and A. Graham, "Nuclear Snake-Arm Robots," *Industrial Robot: An International Journal*, vol. 39, No.1, pp. 6-11, 2012.
- [2] R. Buckingham, V. Chitrakaran, R. Conkie, G. Ferguson, A. Graham, A. Lazell, M. Lichon, N. Parry, F. Pollard, A. Kayani, M. Redman, M. Summers, and B. Green, "Snake-Arm Robots: A New Approach to Aircraft Assembly," in *SAE Aerotech Congress*, Los Angeles, CA, USA, 2007.
- [3] W. Xu, T. Liu, and Y. Li, "Kinematics, Dynamics, and Control of a Cable-Driven Hyper-Redundant Manipulator," *IEEE/ASME Transactions on Mechatronics*, vol. 23, No.4, pp. 1693-1704, Aug 2018.
- [4] H. Lee, K. G. Kim, J. H. Seo, and D. K. Sohn, "Natural Orifice Transluminal Endoscopic Surgery with a Snake-Mechanism Using a Movable Pulley," *The International Journal of Medical Robotics and Computer Assisted Surgery*, vol. 13, No.4, p. e1816, Dec 2017.
- [5] V. C. Anderson and R. C. Horn, "Tensor Arm Manipulator." vol. 3,497,083, U. S. P. Office, Ed. United States, 1970.
- [6] E. Paljug, T. Ohm, and S. Hayati, "The JPL Serpentine Robot: a 12 DOF System for Inspection," in *IEEE International Conference on Robotics and Automation (ICRA)*, Washington, DC, 1995, pp. 3143-3148.
- [7] A. Wolf, H. B. Brown, R. Casciola, A. Costa, M. Schwerin, E. Shamas, and H. Choset, "A Mobile Hyper Redundant Mechanism for Search and Rescue Tasks," in *IEEE/RSJ International Conference on Intelligent Robots and Systems (IROS)*, Las Vegas, Nevada, 2003, pp. 2889-2895.
- [8] H. B. Brown, M. Schwerin, E. Shamas, and H. Choset, "Design and Control of a Second-Generation Hyper-Redundant Mechanism," in *IEEE/RSJ International Conference on Intelligent Robots and Systems (IROS)*, San Diego, CA, USA, 2007, pp. 2603-2608.
- [9] S. Hirose and S. Ma, "Coupled Tendon-Driven Multijoint Manipulator," in *IEEE International Conference on Robotics and Automation (ICRA)*, Sacramento, CA, USA, 1991, pp. 1268-1275.
- [10] G. Endo, A. Horigome, and A. Takata, "Super Dragon: A 10-m-Long-Coupled Tendon-Driven Articulated Manipulator," *IEEE Robotics and Automation Letters*, vol. 4, No.2, pp. 934-941, 2019.
- [11] L. Tang, J. Wang, Y. Zheng, G. Gu, L. Zhu, and X. Zhu, "Design of a Cable-Driven Hyper-Redundant Robot with Experimental Validation," *International Journal of Advanced Robotic Systems*, vol. 14, No.5, 2017.
- [12] J. Yang, P. Jason, and K. Abdel-Malek, "A Hyper-Redundant Continuous Robot," in *IEEE International Conference on Robotics and Automation (ICRA)*, Orlando, Florida, USA, 2006, pp. 1854-1859.
- [13] W. McMahan, V. Chitrakaran, M. Csencsits, D. M. Dawson, I. D. Walker, B. A. Jones, M. Pritts, D. Dianno, M. Grissom, and C. D. Rahn, "Field Trials and Testing of the OctArm Continuum Manipulator," in *IEEE International Conference on Advanced Robotics (ICAR)*, Orlando, FL, USA, 2006, pp. 2336-2341.
- [14] X. Dong, M. Raffles, S. C. Guzman, D. Axinte, and J. Kell, "Design and Analysis of a Family of Snake Arm Robots Connected by Compliant Joints," *Mechanism and Machine Theory*, vol. 77, pp. 73-91, 2014/07/01/ 2014.
- [15] S. Liu, Z. Yang, Z. Zhu, L. Han, X. Zhu, and K. Xu, "Development of a Dexterous Continuum Manipulator for Exploration and Inspection in Confined Spaces," *Industrial Robot: An International Journal*, vol. 43, No.3, pp. 284-295, 2016.
- [16] X. Dong, D. Axinte, D. Palmer, S. Cobos, M. Raffles, A. Rabani, and J. Kell, "Development Of a Slender Continuum Robotic System For On-Wing Inspection/Repair of Gas Turbine Engines," *Robotics and Computer-Integrated Manufacturing*, vol. 44, pp. 218-229, April 2017.
- [17] S. C. Jacobsen, H. Ko, E. K. Iversen, and C. C. Davis, "Antagonistic Control of a Tendon Driven Manipulator," in *IEEE International Conference on Robotics and Automation (ICRA)*, Scottsdale, AZ, USA, 1989, pp. 1334-1339.
- [18] A. Todtheide, T. Lilge, and S. Haddadin, "Antagonistic Impedance Control for Pneumatically Actuated Robot Joints," *IEEE Robotics Automation Letters*, vol. 1, No.1, pp. 161-168, 2016.
- [19] V. Potkonjak, B. Svetozarevic, K. Jovanovic, and O. Holland, "The Puller-Follower Control of Compliant and Noncompliant Antagonistic Tendon Drives in Robotic Systems " *International Journal of Advanced Robotic Systems*, vol. 8, No.5, pp. 143-155, 2011.
- [20] W. Xu, Z. Mu, T. Liu, and B. Liang, "A Modified Modal Method for Solving the Mission-Oriented Inverse Kinematics of Hyper-Redundant Space Manipulators for On-Orbit Servicing," *Acta Astronautica*, vol. 139, pp. 54-66, 2017.
- [21] D. Palmer, S. Cobos-Guzman, and D. Axinte, "Real-Time Method for Tip Following Navigation of Continuum Snake Arm Robots," *Robotics and Autonomous Systems*, vol. 62, No.10, pp. 1478-1485, 2014.